Further studies of both nuclei have been undertaken at Yale and Freiburg to better understand this situation.

ACKNOWLEDGMENTS

Spin Flip in the Inelastic Scattering of 19.6-MeV Protons from ^{54}Fe and ^{56}Fe †

D. L. Hendrie, C. Glashausser,* J. M. Moss,‡ and J. Thirion§

Lawrence Radiation Laboratory, University of California, Berkeley, California 94720

(Received 14 April 1969)

The spin-flip probability in the excitation of the first 2^+ states in ^{54}Fe and ^{56}Fe has been studied at 19.6 MeV using the $(p, p'\gamma)$ coincidence technique. Differential cross sections have also been measured at this energy. The spin-flip data for ^{54}Fe and ^{56}Fe are quite similar, in contrast to asymmetry data from Saclay which show distinct differences between the two nuclei. Collective-model distorted-wave Born-approximation calculations generally underestimate the magnitude of the spin-flip probability at forward angles and predict too little structure. Simple microscopic-model calculations give improved agreement with the spin-flip data only when the terms arising from spin transfer of 1 are significant. These terms had little effect on the predicted cross sections and asymmetries.

I. INTRODUCTION

$\mathbf{S}$PIN-DEPENDENT effective forces in the inelastic scattering of nucleons are generally not well understood, even phenomenologically. Cross sections $\sigma(\theta)$, asymmetries $A(\theta)$, polarizations $P(\theta)$, and spin-flip probabilities $S(\theta)$ are sensitive to these forces in different ways. They can be written:

$$\sigma(\theta) = \sigma_{++}(\theta) + \sigma_{--}(\theta) + \sigma_{+-}(\theta) + \sigma_{-+}(\theta),$$

$$A(\theta)\sigma(\theta) = \sigma_{++}(\theta) + \sigma_{+-}(\theta) - \sigma_{-+}(\theta) - \sigma_{--}(\theta),$$

$$P(\theta)\sigma(\theta) = \sigma_{++}(\theta) + \sigma_{-+}(\theta) - \sigma_{+-}(\theta) - \sigma_{--}(\theta),$$

$$S(\theta)\sigma(\theta) = \sigma_{+-}(\theta) + \sigma_{-+}(\theta). \tag{1}$$

Here, $\sigma_{+-}(\theta)$, e.g., is the absolute differential cross section for scattering from an initial state with incident-nucleon spin projection $+\frac{1}{2}$ to a final state with outgoing-nucleon spin projection $-\frac{1}{2}$ on the z axis. The quantities $\sigma(\theta)$, $A(\theta)$, $P(\theta)$, and $S(\theta)$ all involve independent combinations of the $\sigma_{ij}(\theta)$ partial cross sections. We report here measurements of the cross section and the spin-flip probability in the excitation of the first 2^+ states in ^{54}Fe and ^{56}Fe. The energy of the incident protons was 19.6 MeV. Existing measure-

ments[1] of the cross sections and asymmetries for these two nuclei showed interesting and unexplained differences at 18.6 MeV; recent measurements[2] at 19.6 MeV confirm these differences. Our theoretical analysis includes the 19.6-MeV asymmetry data as well as the present cross-section and spin-flip results.

The spin-flip probability arises from various interfering processes. A corresponding transfer of spin angular momentum to the target nucleus may occur ($\Sigma=1$), but there are also contributions from phenomena without spin transfer ($\Sigma=0$). The usual macroscopic model involves only $\Sigma=0$ type interactions and predicts similar spin-flip probabilities for transitions in neighboring nuclei. In a more detailed description, e.g., in a microscopic one, all processes may contribute and differences can occur.

The relative spin-flip probability for ^{54}Fe has been measured before, at 11 MeV[3]; several isotopes of Cr, Ni, and Zn have also been measured at that energy.[4] The University of Washington group has obtained absolute probabilities for ^{12}C and ^{24}Mg,[5] and they have made an extensive series of measurements on the

* Present address: Rutgers—The State University, New Brunswick, N.J.
‡ Present address: Centre d'Etudes Nucléaires, Saclay, France.
§ Permanent address: Centre d'Etudes Nucléaires, Saclay, France.

[1] C. Glashausser, R. de Swiniarski, J. Thirion, and A. D. Hill, Phys. Rev. **164**, 1437 (1967).
[2] B. Mayer and J. Thirion (private communication).
[3] R. Ballini, N. Cindro, J. Dalaunay, J. Fouan, M. Loret, and J. P. Passerieux, Nucl. Phys. **A97**, 561 (1967).
[4] F. G. Perey, in *Proceedings of the Second International Symposium on Polarization Phenomena of Nucleons, Karlsruhe, 1965*, edited by P. Huber and H. Schopper (Birkhäuser Verlag, Basel, 1966), p. 200.
[5] F. H. Schmidt, Ronald E. Brown, J. B. Gerhart, and Wojiech A. Kolasinski, Nucl. Phys. **52**, 353 (1964).

nickel isotopes at energies from 10–15 MeV.[6] A measurement on ^{58}Ni at 20 MeV has recently been reported.[7] The experiments at energies below 20 MeV do reveal rather large differences among the nuclei studied, but these cannot be directly attributed to a failure of the macroscopic model since compound-nucleus contributions are apparently important. Measurements on ^{12}C and ^{28}Si at energies between 25 and 42 MeV have also been reported.[8,9]

All these measurements, including the present one, use the $(p, p'\gamma)$ correlation method first explored by Schmidt et al.[5] When the γ detector is placed along the normal to the reaction plane defined by the incoming and outgoing protons, coincident protons and γ rays of the appropriate energy define excitation of only the $m = \pm 1$ magnetic substates of the 2^+ state. (The z axis is chosen along the normal to the reaction plane.) From the Bohr theorem[10] it follows that the spin of the incident and outgoing particles are opposite, i.e., that spin flip has occurred.

The experimental method is discussed in detail in Sec. II. The results of the experiment are presented in Sec. III together with a discussion of the errors involved. These results are analyzed in Sec. IV via both macroscopic and microscopic models. Section V is a summary with concluding remarks.

II. EXPERIMENTAL METHODS

The spin-flip experiment was performed in a cave which is presently set up specifically for experiments involving γ-ray detection. The beam from the Berkeley 88-in. Cyclotron was focused by a quadrupole doublet and bent 56° by a switching magnet onto a set of vertical and horizontal slits (the analyzing slits) in the cylotron-vault area. The analyzing power of the switching magnet gave a beam resolution of about 15 keV. The beam then passed through an 8-ft concrete and iron shielding wall, was bent another 12° and finally focused at the target by a second quadrupole doublet; the beam spot was 1.5 mm wide and 3 mm high. Only the analyzing slits were used to define the beam. We chose to use a 39.2-MeV H_2^+ beam to obtain 19.6-MeV protons so that particles scattered from the analyzing slits would be deflected away from the target area by the second bending magnet.

The scattering chamber was a rectangular aluminum box 24 in. long and 8 in. wide and deep with a removable lid. The beam passed close to a thin (75 μ) tantalum window along one side of the box. A Faraday cup which was split vertically along its center line was used to monitor the beam current and alignment. Equal currents were maintained in each half of the Faraday cup to insure a constant position of the beam

spot. The beam position on the target was periodically checked with the aid of a thin scintillating target and a closed-circuit television system. The Faraday cup, which was 7 ft from the target, was shielded by a 30×36-in. aluminum cylinder; the cylinder was lined with a cadmium sheet and filled with borated paraffin. The end of the shield near the scattering chamber was faced with 4 in. of lead.

The targets were evaporated self-supporting isotopically enriched metallic foils of ^{54}Fe and ^{56}Fe. Various targets were used with thicknesses ranging from 200 to 800 $\mu g/cm^2$. The only significant contaminants were carbon and oxygen, which could be readily identified. Four targets were mounted on a wheel; each could be rotated about the beam center line in both the horizontal and vertical planes to any desired angle.

The γ rays were detected with a 40-cm^3 coaxial germanium detector, positioned so that the axis of symmetry passed through the beam spot on the target. This was defined as the z axis of the correlation. Most of the results were obtained with the midplane of the counter 12 cm from the target, although a few runs were taken at smaller and greater distances. The best resolution achieved in prerun tests was 3.8 keV for ^{60}Co, but the resolution obtained during the actual experiment was about 6 keV due to high counting rates ($\sim$20 000 counts/sec). No gain shifts as large as 1 keV were observed during the experiment.

The γ detector viewed the target through the 75-μ tantalum chamber window mentioned previously; in addition a 1-mm tantalum absorber was placed between the target and detector for preferential absorption of low-energy γ rays. The absolute efficiency of the detector was measured in the actual experimental configuration by inserting radioactive sources in the target holder. For this purpose we used a set of calibrated γ sources obtained from the International Atomic Energy Agency. The solid-angle efficiency factor for the full-energy peak was measured to be 2.62×10^{-4} for ^{54}Fe and 4.25×10^{-4} for ^{56}Fe. (This corresponds to detector efficiencies of about 6 and 10%, respectively.) The half-angle subtended by the midplane of the detector was about 7.5°.

Two independently movable particle counters were used, one above, and one below the beam line and both arranged so that the planes defined by the center of the proton counters and the beam axis were perpendicular to the axis of the γ detector. The counters were 3-mm-thick Si(Li) detectors, cooled to about $-40°C$ by flexible straps connected to a liquid-nitrogen cold finger. An aluminum absorber (12 μ) was placed in front of each counter to stop knock-on electrons and to reduce the light sensitivity of the counters. Counter collimators of dimension 0.188×0.239 in. were located 1.2 in. from the center of the target. The dimensions correspond to a solid angle of 0.02 sr and scattering acceptance angles of 11.4° in the scattering plane and 5.6° perpendicular to it (in the z direction). Using both
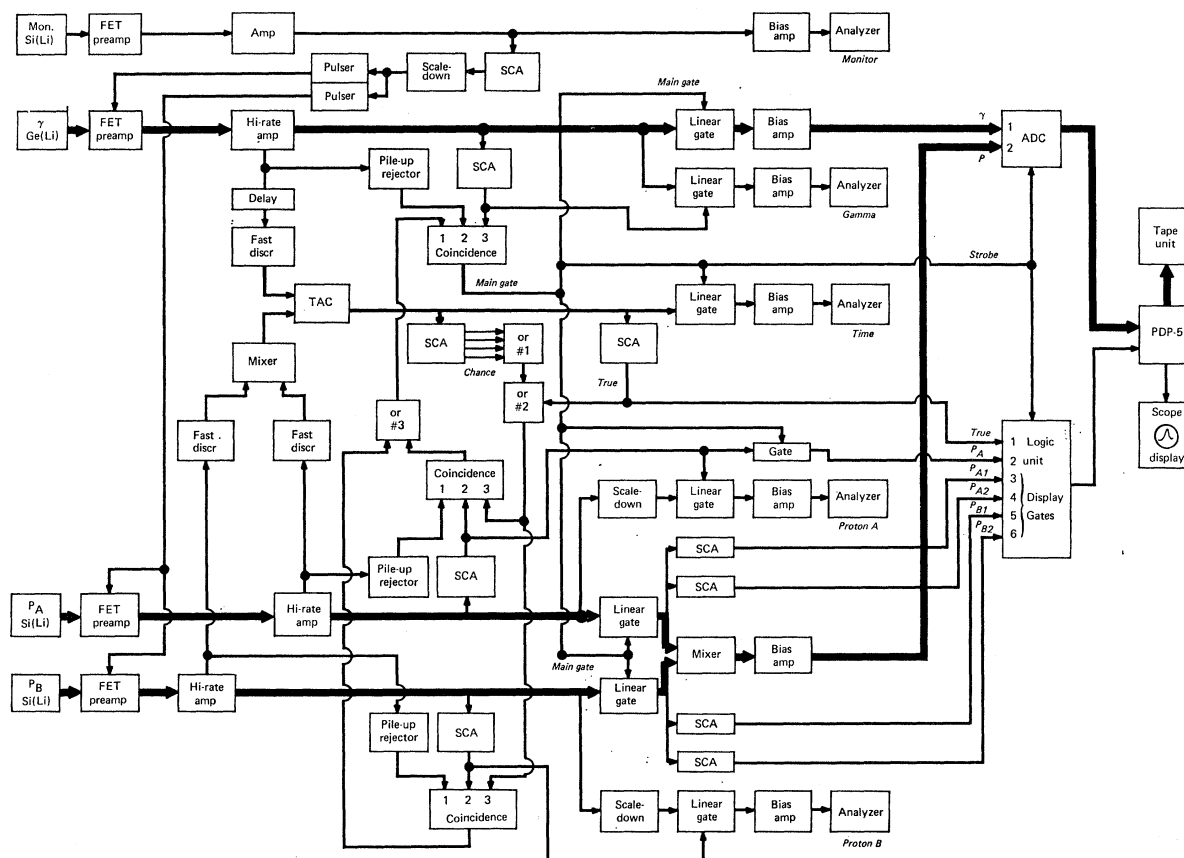
[6] W. A. Kolasinski, thesis, University of Washington, 1967 (unpublished).

[7] J. Eenmaa, F. H. Schmidt, and J. R. Tesmer (to be published).

[8] R. O. Ginaven, E. E. Gross, J. J. Malanify, and A. Zucker, Phys. Rev. Letters 21, 552 (1968).

[9] J. J. Kolata and A. Galonsky, Bull. Am. Phys. Soc. 12, 501 (1967).

[10] A. Bohr, Nucl. Phys. 10, 486 (1959).

FIG. 1. Simplified block diagram of the electronics. The heavy lines indicate the paths of the analog signals from the two proton counters and the γ counter.

counters, the angular range from 35°–150° could be covered; the range from 90°–95° was accessible to both counters for purposes of checking efficiencies. The experimental resolution at counting rates from 8000 to 20 000 counts/sec was 100 keV; most of this was due to kinematic broadening.

A. Electronics

A simplified block diagram of the electronics system is shown in Fig. 1. The central feature is the high-rate amplifier system for each counter. These systems, designed by Goulding, Landis, and Pehl,[11] consist of a high-rate preamplifier, a high-rate linear amplifier employing pole-zero cancellation, a pile-up rejector, and a linear gate. The linear amplifier produces a fast output (~50 nsec rise time) for fast timing and pile-up rejection purposes, and a slow output for energy analysis. The slow output has an approximately Gaussian shape which has a rise time of 3 μsec for the germanium detector and 1 μsec for the particle detectors. The pile-up rejector eliminates any signal whose height is changed because another signal is detected almost in coincidence with it. Pulses which are not discarded

[11] F. S. Goulding, D. A. Landis, and R. H. Pehl, University of California Lawrence Radiation Laboratory Report No. UCRL-17560 (unpublished).

produce a "valid out" signal which, in the present system, is combined with the total coincidence signal to open the linear gate for both γ and proton signals.

The fast outputs of the linear amplifiers were amplified further, shaped, and fed into fast discriminators. The outputs of the two proton fast discriminators were mixed and used to provide a start pulse for a time-to-amplitude converter (TAC); the stop pulse was provided by a similar signal from the γ counter. The
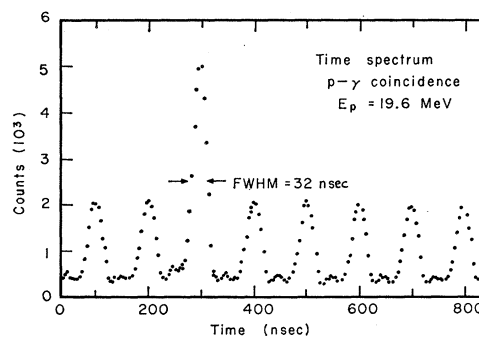

FIG. 2. Pulse-height spectrum from the TAC. The start pulse came from a proton fast discriminator; the stop pulse came from the γ fast discriminator. The SCA's were set so that $0.40 < E_\gamma < 3.5$ MeV. The large peak is the true peak; the other peaks correspond to chance coincidences.

output of the TAC was amplified, fed through a linear gate, and stored in a 400-channel analyzer. The TAC was operated on a 1-μsec time scale; since the cyclotron frequency was about 10 MHz, its spectrum showed 8 and 9 well-separated peaks. One of these (the "true" peak) contained true and chance events; the other contained only chance events (Fig. 2). The total time resolution was about 32 nsec [full width at half-maximum (FWHM) of one of the peaks]. In order to convey the information of the TAC spectrum to the triple slow coincidence, single channel analyzers (SCA's) were set about the true peak and four of the chance peaks. The outputs were then mixed through "OR" circuits to provide the time input to the slow coincidence unit. Additional inputs were provided by SCA's set to encompass the regions of interest in the proton and γ spectra, and by valid output signals from the pile-up rejectors. When all of the criteria were met, viz, SCA and pile-up rejector for either of the proton counters and for the γ counter and a time signal from one of the five selected intervals, a main-gate output opened the linear gate for the γ, proton, and time signals. To insure proper overlap of the input signals to the slow coincidence, all the SCA outputs were timed by strobes from the fast discriminators. Scalers were used to monitor various points of the circuit.

Valid pairs of γ and proton signals were fed into a multiplexed 4096-channel successive-approximation analog-to-digital converter (ADC).[12] In addition, logic signals were provided which identified the proton counter producing the event and which characterized the event as occurring in the true peak or in a chance peak. The analog and logical information was sent via an interrupt mode into a storage buffer in an on-line PDP-5 computer. During the period of digitization and storage (about 400 μsec), an inhibit gate prevented opening of the main gate. After each 1250 events the data buffer was emptied onto magnetic tape.

It was essential to be able to monitor the progress of the experiment in order to insure the proper functioning of all parts of the system and to determine when enough data had been collected. To accomplish this, four additional logic signals were generated by SCA's set about the elastic and first excited-state energy peaks for both proton counters. The four γ spectra specified by these logic signals were generated and separately stored by the on-line computer program and were displayed on an oscilloscope. A light pen was used to extract portions of these display spectra.

In order to normalize the coincidence data, it was necessary to preserve the noncoincidence (singles) proton spectra. This was done by providing secondary branches in the circuit for the proton signals. These signals were scaled down by a factor of 5–50, depending on the counter angle, to provide suitable counting rates for storage in the 400-channel analyzers.

A monitor proton counter was used as a check on the

---

[12] L. B. Robinson, F. Gin, and F. S. Goulding, Nucl. Instr. Methods **62**, 237 (1968).

beam integration. In addition, the elastic peak in this spectrum was scaled down by a factor of 100–1000 and used to trigger a pulser; hence, the frequency of the pulser was proportional to the beam intensity. This pulser then fed accurately timed pairs of pulses to the proton and γ preamp inputs. These pairs of pulses passed through the entire circuit in the same manner as real coincidence events and were stored on tape as such. The pulser voltages were selected in such a way as to overlap with no proton counts (the pulser peak was slightly above the elastic peak) and few γ counts (the pulser peak was set at the high-energy end of the spectrum). Drifts of the pulser voltages would have indicated gain shifts of the electronics, but none were found. More importantly, the number of observed pulser events stored in the two-dimensional array was a direct measure of the dead-time and pile-up losses in the entire system. Since these losses were usually about 40–50% of the input counts, it was crucial to know this quantity precisely. At a γ counting rate of 2×10^4 counts/sec, 70% of these losses came from γ pile-up rejection, $\sim$20% from proton pile-up rejection, $\sim$8% from the TAC, and $\sim$2% from the ADC.

In order to perform the analysis of the coincidence experiment, a run was taken to obtain differential cross sections for ^{54}Fe and ^{56}Fe at 19.6 MeV with good resolution and geometry. Two 3-mm-thick Si(Li) detectors were used; they were cooled to $-35°C$ by thermoelectric devices and equipped with electrostatic electron-suppression plates. The two counters subtended solid angles of 1.7×10^{-4} sr and yielded resolutions of 30 keV. The total beam was measured in a Faraday cup and checked with a fixed position monitor. The total absolute error in extracting the elastic and inelastic cross section is estimated to be less than 10%; the largest uncertainty is due to measurement of the target thickness. Relative errors are less than 2%.

III. DATA REDUCTION AND RESULTS

The number of coincident counts (R) can be related to the spin-flip probability $S(\theta)$ by the following expression in the limit of infinitesimal solid angle:

$$S(\theta) = W(e\Omega_\gamma/4\pi)R/N, \qquad (2)$$

where θ is the proton scattering angle, e is the γ-detector efficiency, Ω_γ is the solid angle subtended by the γ detector, W is a calculable geometrical factor which is equal to $\frac{5}{2}$ for a point counter, and N is the total number of counts in the particle counter arising from excitation of the 2^+ state. In pratice this expression becomes

$$S(\theta) = W(e\Omega_\gamma/4\pi)[(T-C/a)/N] - B(\theta), \quad (3)$$

where T is the measured number of counts in the true time peak, C is the measured number of chance counts and a is the relevant scaling factor between T and C. The contribution due to non-spin-flip processes which arises from the finite solid angles used is labeled $B(\theta)$. Assuming Poisson distributions, the statistical error
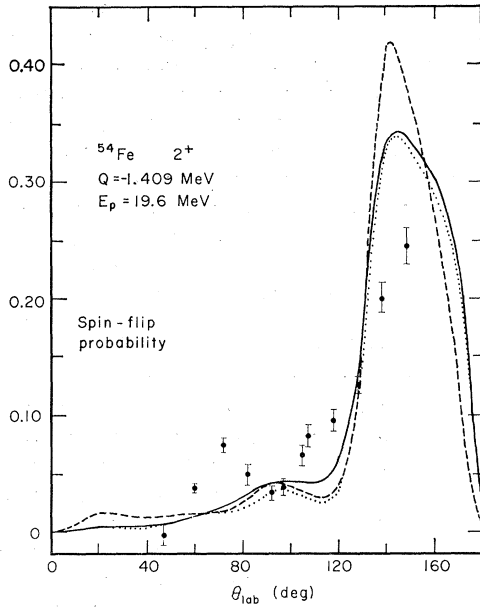
FIG. 3. Spin-flip probability $S(\theta)$ for ^{54}Fe. The curves are collective-model DWBA predictions with three types of spin-orbit terms: Full Thomas term (solid); $U(1)$ only, Eq. (7a), (dotted); and nondeformed spin-orbit (dashed).

associated with each datum is then

$$[\delta S(\theta)]^2 \approx \left[W\left(\frac{e\Omega_\gamma}{4\pi}\right) \right]\left[T + \frac{C}{a^2} + \frac{C^2(\delta a)^2}{a^4} \right] \Big/ N; \qquad (4)$$

this is the error we will quote. The statistical errors in the other measured quantities, such as e or N, are not significant; the errors were almost invariably dominated by the error in T.

Two different procedures were used to evaluate the number of coincidence events, T or C. The first was to sum over a small region of the two-dimensional array that contained only the 2^+ proton peak and the full-energy γ peak (FEP). The efficiency of the γ detector could be directly interpolated from our calibration curve. The second procedure included γ counts in the
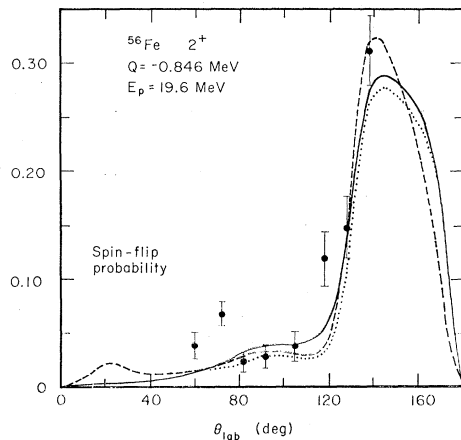

FIG. 4. Spin-flip probability $S(\theta)$ for ^{56}Fe. The curves are collective-model DWBA predictions as described for Fig. 3.
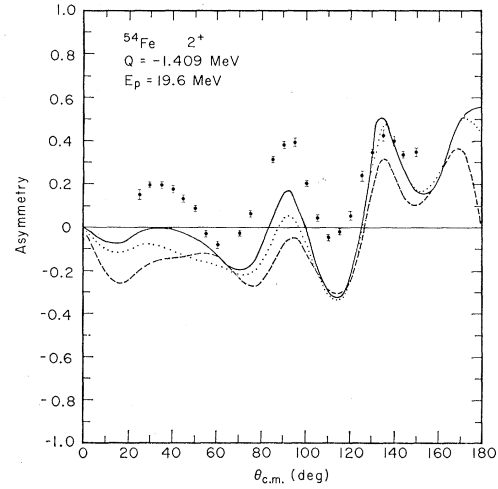

FIG. 5. Asymmetry for ^{54}Fe, measured at Saclay (Ref. 2). The curves are collective-model DWBA predictions as described for Fig. 3.

FEP and Compton distribution down to, but not including, the annihilation peak at 511 keV. The efficiency for this method of summation was obtained in the following way. The total number of counts (R) in coincidence with the 2^+ proton peak was evaluated for each method of summation. Then these quantities were summed over all angles in order to obtain the ratio of the total number of counts in the Compton + FEP region to those in the FEP alone. This results in a 5% statistical error in the over-all normalization.

The full spectrum summation increases the efficiency by a factor of 8.5 for the 1.409-MeV state of ^{54}Fe. The final results are obtained by this method. Comparison of the two methods for ^{54}Fe showed,
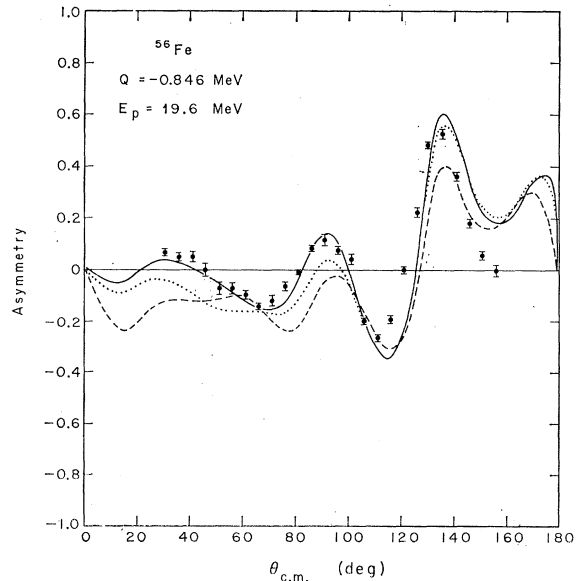

FIG. 6. Asymmetry for ^{56}Fe, measured at Saclay (Ref. 2). The curves are collective-model DWBA predictions as described for Fig. 3.

within errors, the same results. For ^{56}Fe, the summations were over only the FEP.

Alternative procedures were available for obtaining C, the number of chance counts. The most straightforward was to sum the number of counts in coincidence with the *elastic* proton events over the same γ-energy region as for the real events. The scale factor a determined in this way is just the ratio of noncoincident elastic to inelastic proton events. It was usually statistically advantageous, however, to obtain C exactly as for T but from the four time-delayed chance peaks. However, due to very rapid beam-intensity fluctuations (microstructure), a was not 4, but varied from 3.6–3.9. The value of a was determined by summing the γ spectrum in coincidence with elastic events from 520 keV to above the FEP. Again, the comparison of these two methods yields statistically identical results. The singles proton spectra, scaled down to eliminate analyzer dead-time effects, were recorded for both counters in all runs. At forward and backward angles, the number of singles events could be extracted directly from these spectra. At intermediate angles, the 2^+ peak was obscured by elastic events from carbon and oxygen target contaminants. At these angles, the ratio between inelastic and elastic events was determined from the previously measured cross sections by averaging over the angular acceptance of the proton counters. Where it was possible to check, this indirect method agreed with the direct determination to within 10%.

The admixture of the non-spin-flip contribution $B(\theta)$ was calculated to be generally about 0.02 if the reasonable assumption was made that all such amplitudes are equally probable and that coherent effects were small. Maximum violation of these assumptions would change $B(\theta)$ by less than a factor of 2. At two angles (45° and 95°) for ^{54}Fe, $B(\theta)$ was directly measured by both increasing and decreasing the γ-
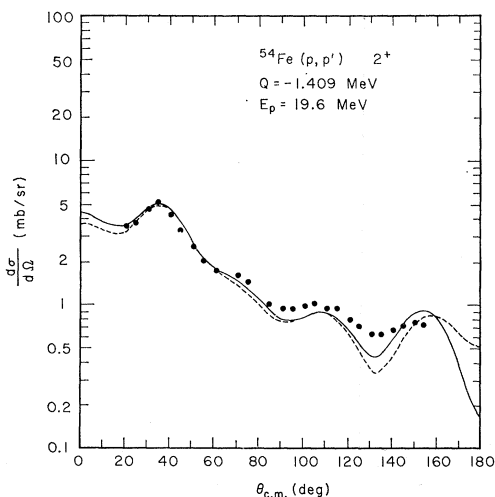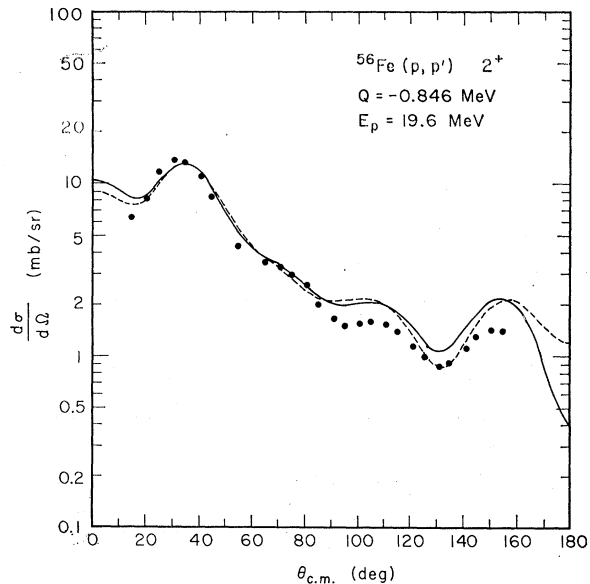

FIG. 8. Differential cross section for ^{56}Fe. The curves are collective-model DWBA predictions as described for Fig. 3.

counter solid angle by a factor of 2. These measurements are consistent within statistics with the calculation.

The values of $S(\theta)$ for the first 2^+ states of ^{54}Fe and ^{56}Fe are shown in Figs. 3 and 4 along with theoretical predictions which will be discussed later. It is apparent that the large differences between the asymmetries for the two states are not reflected in these data. In addition to the large angle peak also seen in other work,[3–9] both distributions show a maximum at 70°; these features are more pronounced in ^{54}Fe where the statistical precision is better.

Figures 5 and 6 show the asymmetries for the first 2^+ states of ^{54}Fe and ^{56}Fe, respectively, obtained with 19.6-MeV polarized protons at Saclay.[2] These data are quite similar to those measured at 18.6 MeV,[1] suggesting that compound-nucleus contributions are not important. The small asymmetry at 30° and 90° for ^{56}Fe is found also for $L=2$ transitions in the nickel isotopes, whereas large asymmetries at these angles were observed[1] for ^{52}Cr and ^{50}Ti.

Cross sections for the two states in ^{54}Fe and ^{56}Fe also have different shapes; they are shown in Figs. 7 and 8. The cross section for ^{54}Fe decreases less rapidly with increasing angle than does the ^{56}Fe cross section.

IV. ANALYSIS

A. Optical Model

The predictions of $S(\theta)$ in a collective-model analysis are quite sensitive to the optical parameters chosen, in particular, to the depth of the spin-orbit potential and to a lesser extent to the parameters of the imaginary potential. For this reason we have made a rather extensive search of parameter space to determine the

FIG. 7. Differential cross section for ^{54}Fe. The curves are collective-model DWBA predictions as described for Fig. 3.

TABLE I. Best-fit optical-model parameters for ^{54}Fe and ^{56}Fe.

	V (MeV)	W_D (MeV)	V_{so} (MeV)	r_r (F)	r_i (F)	r_{so} (F)	a_r (F)	a_i (F)	a_{so} (F)
^{54}Fe	50.51	7.94	5.06	1.19	1.31	1.075	0.70	0.55	0.40
^{56}Fe	50.48	8.83	5.12	1.19	1.31	1.075	0.70	0.55	0.40

degree to which the best-fit parameters are fixed on the basis of χ^2. For both nuclei, cross section and polarization data at 19.6 MeV were analyzed.

The optical potential used had the standard form

$$U(r) = -Vf(r, r_r, a_r) - 4ia_iW_D(d/dr)f(r, r_i, a_i)$$
$$+ (\hbar/m_\pi c)^2 V_{so}(l \cdot \sigma)r^{-1}(d/dr)f(r, r_{so}, a_{so}). \quad (5)$$

The Coulomb potential of a uniformly charged sphere was added to $U(r)$; the functions $f(r, r_r, a_r)$ are of the Wood-Saxon form. A modified version of the UCLA code SEEK[13] was used to minimize χ^2 which is defined as

$$\chi^2 = \chi_P^2 + \chi_\sigma^2,$$

where

$$\chi_\sigma^2 = \sum_i \frac{(\sigma_t{}^i - \sigma_{ex}{}^i)^2}{E_i^2}, \quad (6)$$

$$\chi_P^2 = \sum_i \frac{(P_t{}^i - P_{ex}{}^i)^2}{E_i^2}.$$

The subscripts t and ex refer to the values of the theoretical and experimental quantities, respectively, at each point i. The E_i are the experimental errors.

Unless stated otherwise, we have taken the errors to be a constant percentage of the cross section at each angle (usually 3%); for the polarization, the quoted experimental errors were used (ranging from ± 0.01 at forward angles to ± 0.03 at backward angles).

In accordance with previous analyses in this energy region, we have generally used a pure surface imaginary well and only a real spin-orbit well. The addition of a small volume term (1.5 MeV) improves the fit only slightly and has a negligible effect on the inelastic predictions. The imaginary spin-orbit well was found to be close to zero in the analysis of 18.6-MeV elastic scattering[14]; we have found that this remains true at 19.6 MeV and have therefore omitted it in the analysis.

In addition to V, W_D, and V_{so}, the geometrical parameters of all three potentials were used as variables in the fit to the cross-section and polarization data. The usual procedure was to use only a few parameters at a time as variables in order to more easily assess the improvement in the fit due to each.

Several parameters (all except r_s, a_s, V, a) were gridded over a sizable range while χ^2 was minimized at each point. This allowed the explicit χ^2 dependence of the gridded parameter to be displayed and lessened the possibility of missing any local minima.
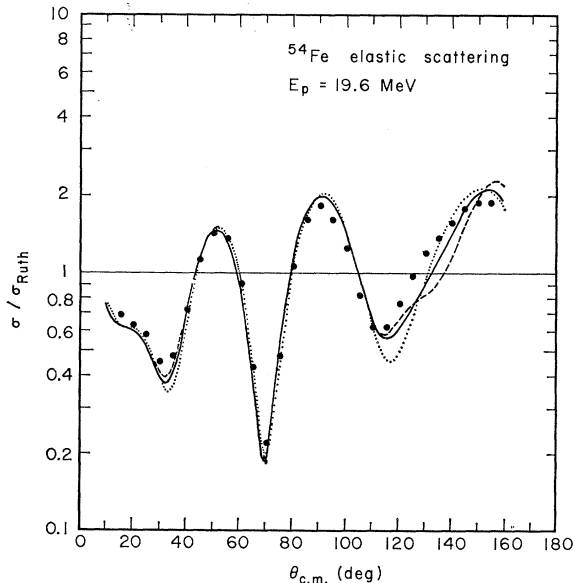

FIG. 9. Ratio of the elastic scattering cross section for ^{54}Fe to the Rutherford cross section. The solid curve is an optical-model fit using the best-fit parameters of Table I. The dotted and dashed curves are fits using the parameters of Table II with V_{so} fixed at 4 and 6 MeV, respectively.
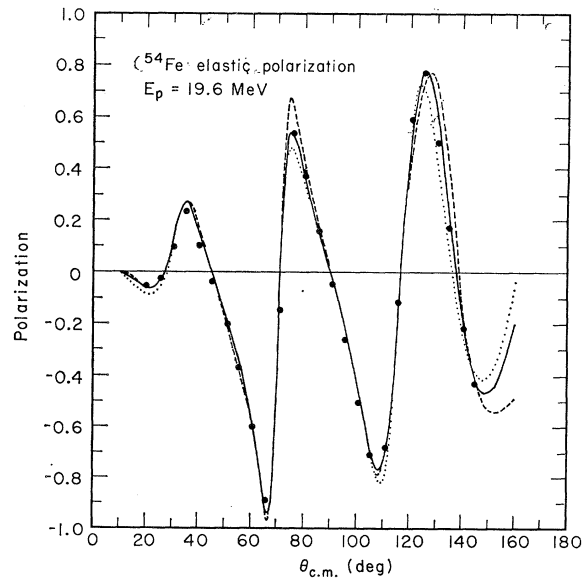

FIG. 10. Polarization in elastic scattering (Ref. 2) from ^{54}Fe. The curves are optical-model fits with the parameters of Tables I and II. The curves are identified in Fig. 9.

[13] M. A. Melkanoff, J. Raynal, and T. Sawada, University of California at Los Angles Report No. 66-10, 1966 (unpublished).

[14] P. Kossanyi-Demay, R. de Swiniarski, and C. Glashausser, Nucl. Phys. A94, 513 (1967); P. Kossanyi-Damay and R. de Swiniarski, ibid. A108, 577 (1967).

TABLE II. Best-fit parameters for ^{54}Fe with fixed V_{so}.

V (MeV)	W_D (MeV)	V_{so} (MeV)	r_r (F)	r_i (F)	r_s (F)	a (F)	a_i (F)	a_{so} (F)
49.89	8.83	4.00	1.19	1.34	1.06	0.73	0.50	0.22
50.51	7.94	5.06	1.19	1.31	1.075	0.70	0.55	0.40
48.82	8.04	6.00	1.22	1.30	1.13	0.66	0.54	0.45

The results of this procedure indicated no significant difference in any of the geometrical parameters between ^{54}Fe and ^{56}Fe; thus we adopted the average set given in Table I. These are close to those used by Kossanyi-Demay and de Swiniarski[14] for the analysis of 18.6-MeV proton scattering. A real radius of 1.19 F seems quite adequate for both nuclei; any restriction of this parameter to values smaller than 1.17 F or larger than 1.25 F results in a considerably poorer fit. The real diffuseness remains close to 0.7 F for a wide variety of parameter situations. An imaginary radius which is larger than the real radius results in a significant improvement in the fit; this is consistent with previous work.[14,15] For the present data, values of at least 1.3 F are required. The diffuseness of the imaginary well is found to be consistently smaller than the real diffuseness. The spin-orbit radius was found to be consistently about 10% less than the real radius in a wide variety of parameter configurations; this, of course, has been observed before.[14,16] The spin-orbit diffuseness is rather poorly fixed between 0.35 and 0.5 F.

Using the average geometrical parameters and searching only on V, W_D, V_{so} we find significant differences

between ^{54}Fe and ^{56}Fe only in the depth of the imaginary potential. The final parameters are given in Table I; the corresponding fits are shown in Figs. 9–12. The polarization data are fit quite well (especially for ^{54}Fe) while the cross-section fits are only fair. It is of interest to note that in the back-angle region, where the fits are poor, there are considerable differences between the ^{54}Fe and ^{56}Fe cross sections. Thus the similarity in optical potentials is somewhat misleading.

Attempts were made to improve the agreement with the back-angle cross-section points by increasing their corresponding weighting factors. However, this decreases the quality of the fit generally and results in only a slight difference in optical parameters.

In parameter searches using only cross-section data, we found that it is possible to obtain quite good fits for both ^{54}Fe and ^{56}Fe if r_i is 1.4 F. This also requires that W_D be about 16 MeV, which is significantly larger than the values found in previous analyses; a_i was usually about 0.35 F. The polarization fits which are produced by such parameters are very poor and allow one to eliminate these solutions. We mention this only to illustrate the dangers of parameter searches using only differential cross-section data.

As we have mentioned, the prediction of $S(\theta)$ in terms of a collective-model (DWBA) analysis is
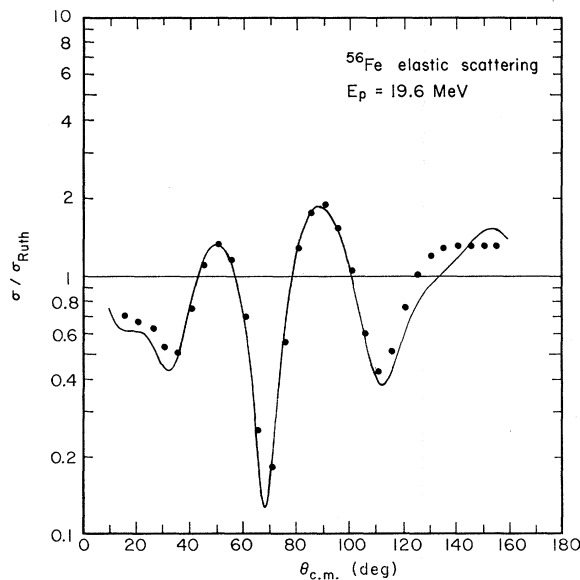

FIG. 11. Ratio of the elastic scattering cross section for ^{56}Fe to the Rutherford cross section. The curve is an optical-model fit with the parameters of Table I.

[15] G. R. Satchler, Nucl. Phys. A92, 273 (1967).
[16] D. J. Baugh, J. A. R. Griffith, and S. Roman, Nucl. Phys. 83, 481 (1966).
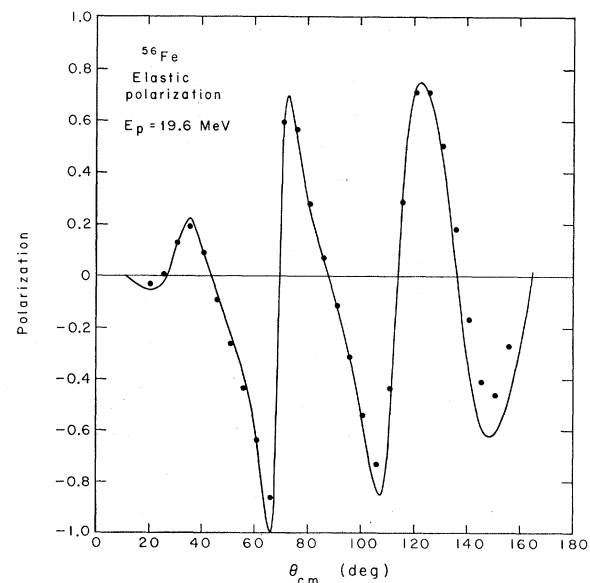

FIG. 12. Polarization in elastic scattering (Ref. 2) from ^{56}Fe. The curve is an optical-model fit with the parameters of Table I.
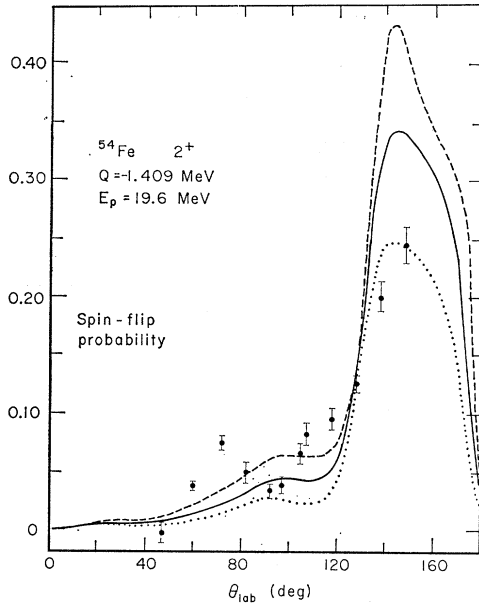
FIG. 13. Collective-model predictions of $S(\theta)$ with the optical parameters of Table II. These were obtained by fixing the spin-orbit well depth at 4 (dotted), 5 (solid), and 6 MeV (dashed).

sensitive to the spin-orbit potential. To examine the extent to which these parameters are determined by the present analysis, we have fixed the well depth V_{so} for ^{54}Fe at 1 MeV on either side of the minimum and searched on all the other parameters. The parameters resulting from this procedure are given in Table II. The corresponding fits to the elastic data for the three spin-orbit well depths are shown in Figs. 9–10. The effect of such parameter adjustments on the predicted inelastic quantities will be discussed in the following section.

B. Collective Model

The collective model has long been used to interpret differential cross sections and polarizations for states assumed to be vibrational. The inelastic transition is considered to be caused by the deformation of the optical potential; deformations of both the real and imaginary potentials are included. It has also been found necessary, in the analysis of asymmetry data,[1,17] to include a deformed spin-orbit term in the interaction. The form of this term is not yet standard.[18]

The most extensive treatment of the spin-orbit deformation has been given by Sherif and Blair.[19] Starting with the Thomas form of the spin-orbit potential which can be derived from the impulse approximation, they show that the resulting deformed

[17] M. P. Fricke, E. E. Gross, and A. Zucker, Phys. Rev. **163**, 1153 (1967).
[18] C. Glashausser and J. Thirion, in *Advances in Nuclear Physics*, edited by M. Baranger and E. Vogt (Plenum Press, Inc., New York, 1969), Vol. II, p. 79.
[19] H. Sherif and J. S. Blair, Phys. Letters **26B**, 489 (1968); H. Sherif, thesis, University of Washington, 1967 (unpublished)

spin-orbit term can be written as follows:

$$U = U(1) + U(2) \qquad (7)$$

where

$$U(1) = (\hbar/m_\pi c)^2 V_{so} I(\theta, \phi) r^{-1} (\partial/\partial r)(\partial f/\partial R_{so})(\boldsymbol{\sigma}\cdot\mathbf{l}), \quad (7')$$

$$U(2) = (\hbar/m_\pi c)^2 V_{so}(\partial f/\partial R_{so})\boldsymbol{\sigma}\cdot[\nabla I(\theta, \phi)\times i^{-1}\nabla]. \quad (7'')$$

R_{so} and $I(\theta, \phi)$ are parameters of the deformed spin-orbit potential

$$R_{so}(\theta, \phi) = R_{so}{}^0 + I(\theta, \phi), \qquad (8)$$

$$I(\theta, \phi) = R_{so}{}^0 \sum_{\lambda\mu} \alpha_{\lambda\mu} Y_{\lambda\mu}(\theta, \phi), \qquad (9)$$

and

$$f = [1 + \exp(r - R_{so}/a_{so})]^{-1}. \qquad (10)$$

The term $U(2)$ contains nonradial components of the gradient operator and is quite complicated to evaluate. For this reason, earlier analyses[1,17] using a deformed spin-orbit potential neglected $U(2)$. In the model of Sherif and Blair, the effects of both $U(1)$ and $U(2)$ are included; i.e., the full Thomas term is used.

For the analysis of the data, a computer program written by Sherif which includes the effects of deformation of the entire optical potential was used. For the spin-orbit deformation, options were available for using the full Thomas term (FT), $U(1)$ deformation only, or a nondeformed spin-orbit potential (NDSO). Coulomb excitation was included in all calculations.

Figures 3 and 4 show the collective-model fits to $S(\theta)$ for the first 2^+ states of ^{54}Fe and ^{56}Fe using the optical parameters in Table I. For these data, no one of
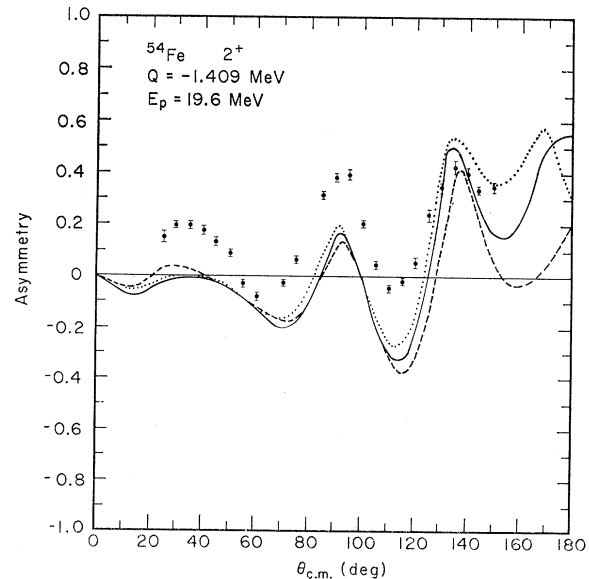

FIG. 14. Collective-model predictions of the asymmetry with the optical parameters of Table II. The curves are identified as in Fig. 13.

the three types of spin-orbit deformation is clearly preferred. For ^{54}Fe all give a rather rough account of the data [i.e., they predict large $S(\theta)$ at back angles] but none fit well. There is some improvement in the predicted magnitude of the back-angle peak when one includes a deformed spin-orbit term. For ^{56}Fe the fit is somewhat better, particularly at back angles. For both nuclei, however, all predictions fail to account for an additional peak at 70°.

The fits to the asymmetries for these states are shown in Figs. 5 and 6. The fit to the ^{54}Fe data is poor; however, a substantial improvement is made by the inclusion of a deformed spin-orbit term, and even further improvement is obtained when the FT term is used. The three types of calculations for the ^{56}Fe asymmetry, are nearly identical to those for ^{54}Fe. In this case, however, the measured asymmetries are smaller and the FT calculations produces a quite good fit. Similar results were obtained at 18.6 MeV where the ^{54}Fe asymmetry was fitted poorly and the ^{56}Fe asymmetry was fitted rather well.[1]

The fits to the differential cross sections are shown in Figs. 7 and 8. In general, these predictions show little sensitivity to the spin-orbit deformation. Again there is the problem of fitting experimental distributions which are rather different with theoretical curves which are quite similar. It is seen that the phase is predicted well but the decrease of the cross section with angle is fitted poorly in both cases.

In order to determine to what degree the collective-model predictions are made ambiguous by uncertainties in the spin-orbit potential, we show the inelastic predictions with the optical parameters of Table II in Figs. 13–15; these were calculated with the spin-orbit strength for ^{54}Fe fixed at 4, 5, and 6 MeV. The predicted $S(\theta)$ is very sensitive to V_{so}; this has been observed in previous work on ^{58}Ni.[7] The solution

FIG. 16. Microscopic model predictions of $S(\theta)$ for ^{54}Fe. For all these curves, $V_0=V_1=-65$ MeV. The ground state was assumed to be $(f_{7/2})^2{}_{0^+}$. The 2^+ state was assumed to be: $(f_{7/2})^2{}_{2^+}$ (solid curve) $(f_{7/2}, f_{5/2})_{2^+}$ (dashed curve) $(f_{7/2}, p_{3/2})_{2^+}$ (broken curve), $\{0.707 \ (f_{7/2})^2{}_{2^+}+0.707 \ (f_{7/2}, p_{3/2})_{2^+}\}$ (dotted curve), $\{0.707 \ (f_{7/2})^2{}_{2^+}-0.707 \ (f_{7/2}, p_{3/2})_{2^+}\}$ (dot-dashed curve).

with $V_{so}=4$ MeV agrees with the data at back angles but fails elsewhere. For the cross-section and asymmetry predictions there is little difference among them.

The calculated values of $S(\theta)$ are less sensitive to the imaginary potential. Calculations for ^{54}Fe were performed with two sets of optical parameters with W_D fixed at 7 and 9 MeV, respectively. The chief difference between the two predictions is in the back-angle maximum which decreases from 0.36 to 0.32.

C. Microscopic Model

The simplified nucleon-nucleon interaction which has normally been used in microscopic-model calculations[20] includes a spin-dependent term which can induce transitions with $\Sigma=1$. The interaction is written:

$$V(r_{ij}) = (V_0+V_1\boldsymbol{\sigma}_i\cdot\boldsymbol{\sigma}_j)g(|\ r_{ij}\ |). \qquad (11)$$

In the present calculations, $g(|\ r_{ij}\ |)$ was assumed to be of Gaussian form with a range of 1.85 F. The sign and strength of V_1 in this effective interaction are not well established. If it is large enough, and $\Sigma=1$ transfer is important, the poor results of the collective-model treatment described above might be explained. If only $\Sigma=0$ excitations are important, previous work indicates that this version of the microscopic model cannot explain the differences in asymmetries and cross sections for ^{54}Fe and ^{56}Fe. Because the wave functions of the two states are not known, however, only simple configurations were considered.[1]
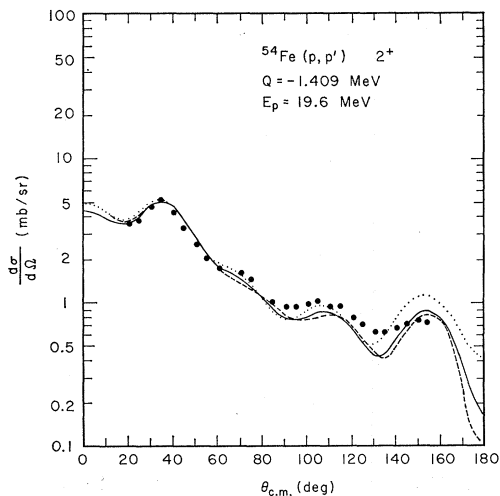

FIG. 15. Collective-model predictions of the differential cross section with the optical parameters of Table II. The curves are identified as in Fig. 13.
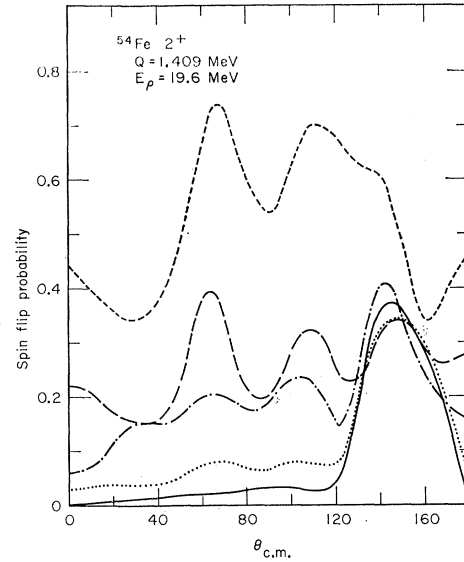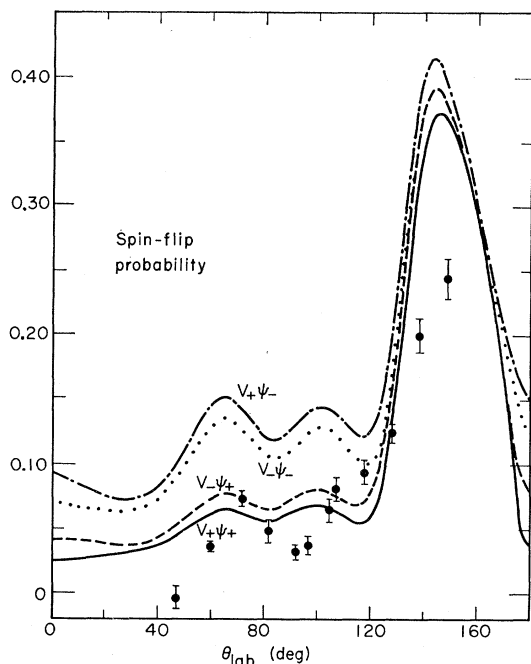
---

[20] N. K. Glendenning and M. Veneroni, Phys. Rev. 144, 839 (1966); G. R. Satchler, Nucl. Phys. 77, 481 (1966).

The predictions of the asymmetries and cross sections show a less marked, but still definite dependence on the configurations assumed and on the magnitude of V_1. Calculations of $S(\theta)$ for these same transitions with V_1 set to zero resemble the collective-model predictions and depend little on the configuration. In this case, the asymmetry and cross section are more configuration-dependent than $S(\theta)$.

Examples of calculations with V_1 set to the more typical value of 30 MeV are shown in Fig. 17. The 2^+ wave function here has been assumed to have components $0.707(f_{7/2})_{2^+}^2$ and $0.707(f_{7/2}, f_{5/2})_{2^+}$. The ground state was pure $(f_{7/2})_{0^+}^2$. Particle wave functions were used instead of hole wave functions for convenience. Calculations with admixtures of other configurations give similar results. The predicted values of $S(\theta)$ are now smaller at forward angles as a result of the reduction in strength of V_1. The four curves in Fig. 17 illustrate the effects of changing the relative sign of the two components of the wave function and the sign of V_1. The positive sign in the wave function increases the predicted value of $\sigma(\theta)$, i.e., this choice leads to collective enhancement. It corresponds to the two lower curves in Fig. 17. The smaller values of $S(\theta)$ reflect mainly the larger values of $\sigma(\theta)$, because most of the collective enhancement occurs in $\sigma_{++}(\theta)$ and $\sigma_{--}(\theta)$, the non-spin-flip terms. Although none of these choices provide a good fit to the asymmetry data, the choice of a positive V_1 and a positive relative sign in the wave function seems slightly favored. The cross section and asymmetry fits thus select the lowest $S(\theta)$ curve. Since realistic wave functions for ^{54}Fe are not available, it did not appear useful to attempt a detailed fit to the experimental $S(\theta)$ by
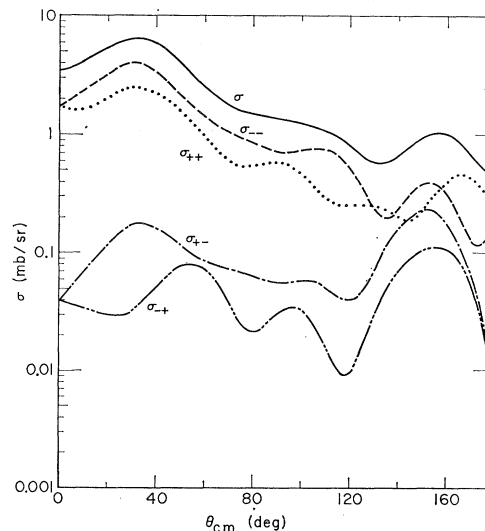

F FIG. 17. Microscopic model predictions of $S(\theta)$ for ^{54}Fe. For these curves V_0 is -65 MeV, V_1 is ±30 MeV. The ground state was assumed to be $(f_{7/2})^2_{0^+}$. The 2^+ state was assumed to be:

$$1/\sqrt{2}(f_{7/2})^2_{2^+}\pm1/\sqrt{2}(f_{7/2}, f_{5/2})_{2^+}.$$

The present microscopic analysis is hampered by the same difficulty. Since there are 28 neutrons in ^{54}Fe, the predominant configuration of the first 2^+ state is presumably $(\pi f_{7/2})_{2^+}^{-2}$; other configurations are sufficiently important, however, that the value[21] of $B(E2)$ is almost nine single-particle units. Since $\Sigma=1$ transfer is forbidden in transitions which involve simply recoupling the angular momentum of two nucleons, contributions of $\Sigma=1$ to the excitation of the 2^+ state in ^{54}Fe must come entirely from admixed configurations. These are probably many of the same configurations which predominate in the 2^+ state of ^{56}Fe. There the neutron shell is no longer closed, the energy of the first 2^+ state is lower, and $B(E2)$ is about 14 single-particle units.[21]

In order to estimate the possible effects of $\Sigma=1$ transfer, calculations were first performed for simple particle transitions with V_0 and V_1 both fixed at 65 MeV. They were carried out with the code of Glendenning; harmonic-oscillator wave functions were used for the bound states. Predictions of $S(\theta)$ for ^{54}Fe are shown in Fig. 16. The curve calculated for pure recoupling of $f_{7/2}$ particles resembles the collective-model fit. The other curves clearly show much larger probabilities at forward angles and vary markedly, depending on the configurations. It is interesting that peaks in $S(\theta)$ are generally predicted near 70° and 105°, the location of the small peaks in the measured $S(\theta)$.

[21] P. H. Stelson and L. Grodzins, Nucl. Data **1**, 42 (1965).

FIG. 18. Microscopic predictions of the partial cross sections [cf. Eq. (1)] for ^{54}Fe. For these calculations V_0 is -65 MeV and V_1 is -30 MeV. The wave function is assumed to be:

$$1/\sqrt{2}(f_{7/2})^2_{2^+}+1/\sqrt{2}(f_{7/2}, f_{5/2})_{2^+}.$$

adjusting parameters of the microscopic interaction. Nevertheless Fig. 17 clearly shows the role of $\Sigma=1$ in terms in the forward-angle structure of $S(\theta)$.

The partial cross sections predicted with the above choice of signs are shown in Fig. 18. Inspection of this and several similar plots have led to several general conclusions. The fits to the experimental $\sigma(\theta)$, although slightly dependent on the details of the microscopic calculation, are not, in general, worse than those obtained with the collective model. The spin-flip cross section, not just the probability, is enhanced at back angles. Calculations which include only the $\Sigma=0$ term reduce the spin-flip cross section at forward angles by a factor of 2 or 3, but leave the back-angle peak relatively unaffected. This peak disappears, however, when only $\Sigma=1$ terms are included. The cross section is mostly due to the sum of $\sigma_{++}(\theta)$ and $\sigma_{--}(\theta)$, and the asymmetry is due mainly to the difference between these same two terms. Except for the back-angle peak where the spin-flip and non-spin-flip cross sections are of comparable magnitude, the spin-flip cross sections provide only minor modifications to $\sigma(\theta)$ and $A(\theta)$. Specifically, inclusion of the $\Sigma=1$ terms, although indicated by the small-angle spin-flip data, have no significant effect on $\sigma(\theta)$ and $A(\theta)$.

V. SUMMARY

Spin-flip probabilities and cross sections for the excitation of the first 2^+ states in ^{54}Fe and ^{56}Fe have been measured for inelastic proton scattering at 19.6 MeV. These data and asymmetry data from Saclay have been analyzed with both macroscopic and microscopic DWBA models; neither gives a good account of all the data.

With the collective model, the fits to the differential cross sections are reasonably good; however, the slopes of the curves are different for the two states and these are not reproduced. The differences between the magnitudes of the asymmetries likewise are not reproduced. These failures are not surprising in view of the nature of the collective model. Differences would have to arise from very different optical parameters for the two nuclei and there is no evidence for this in the present analysis. Other analyses[7,8] have shown that the back-angle peak in the spin-flip probability for ^{58}Ni could be reproduced rather well by collective-model DWBA predictions with or without a deformed spin-orbit term. We also find this to be true; however, the back-angle peak in ^{54}Fe is fitted less well than in the other nuclei. In addition, the structure of $S(\theta)$ is more complex than predicted by the collective analysis.

Since accurate wave functions for the two nuclei were not available, the microscopic analysis could only indicate the results which might be expected from a more complete calculation. If the admixtures of configurations other than $(f_{7/2})_{2^+}{}^{-2}$ are sufficiently large, the calculations indicate that $S(\theta)$ at forward angles can be fit with a reasonable choice of V_1. The ratio of V_1/V_0 must be proportionately larger than about 0.5 to have a significant effect on the predicted $S(\theta)$ if, as expected, the $(f_{7/2})_{2^+}{}^{-2}$ configuration has a probability larger than about 0.5, which it had in our sample case. The shape of $S(\theta)$ depends only slightly on the particular configuration admixtures and on their relative phases when the $(f_{7/2})_{2^+}{}^{-2}$ configuration is predominant. However, if other configurations dominate, as would be expected for 2^+ states other than the lowest, and if V_1/V_0 is large enough, then entirely different $S(\theta)$ patterns are predicted. The shapes then depend sensitively on the relative amplitudes and phases of different configurations.

It remains puzzling that the spin-flip probabilities for ^{54}Fe and ^{56}Fe are quite similar, while the asymmetries and cross sections are different. Whatever reaction mechanism or coherence property of the wave functions is responsible for these differences must not affect $S(\theta)$. This might be possible if, e.g., the spherical spin-orbit potential alone could account for the measured $S(\theta)$, but this is not indicated by our analysis. It is also possible, of course, that contributions due to nucleon-nucleon tensor and spin-orbit forces could bring about the required differences. Since these forces, again, affect mostly the σ_{+-} and σ_{-+} terms, our results suggest that they alone would not resolve the puzzle. Calculations which incorporate these forces, and which include space-exchange terms as well, have recently become possible.[22] A comparison of the predictions of such a code with the present results should prove interesting.

[22] R. Ascuitto and J. Hocquenghem (private communication); R. Schaeffer (private communication).